

OPTIMIZED DESIGN FOR A COMPACT LINAC WITH COLLINEAR ABSORBING LOADS AT THE HUST FEL-THz

J. Jiang, T. N. Hu*, G.Y. Feng, Y. Lu, X. D. Tu, Y. Q. Xiong,
Huazhong University of Science & Technology, 430074 Wuhan, China
Y. J. Pei, National Synchrotron Radiation Laboratory, USTC, Hefei, China

Abstract

To meet the requirement of miniaturization for high power THz radiation in the field of commercial and civil use, RF Linacs have been applied widely as beam injectors, and the Linac with collinear absorbing loads reveals the potential to achieve a tradeoff between performance and compactness. Under overall consideration of systematic conflicts, optimization choices for such Linacs involving power absorbing ability, accelerating efficiency, as well as beamline length were described in this context. Meanwhile, cold testing has been conducted to verify design parameters for the collinear absorbing loads. Furthermore, elaborated calculation of thermal power loss and integrated helical water channel cooling has been performed for the 14MeV Linac with collinear absorbing loads installed on the HUST FEL-THz, and online experiments demonstrated that both the accelerating efficiency and the water cooling performance fulfilled operation demands.

INTRODUCTION

In recent decades, a lot of attention has been paid on compact high-power free-electron laser (FEL)-based terahertz (THz) radiation sources, which can be applied to the fields of security, communications and other scientific fields [1,2]. Since Linac-based FEL can provide above megawatt (MW) peak power radiation with the spectrum covering entire THz band [3,4], efforts have been made to reduce the facility scale and simplify peripheral systems.

Huazhong University of Science and Technology has built a prototype of compact FEL-THz facility [5], which has chosen a room-temperature accelerator to provide high-quality electron beams. Similar as typical beam injectors, the HUST-FEL-THz injector consists of a RF gun and a Linac, and the latter is set to boost the beam extracted by the RF gun to an energy of 14MeV. In order to absorb remnant RF power, an output coupler is commonly installed at the termination of the Linac. Since collinear load instead of traditional waveguide load is advanced for Linac miniaturization [6] and field symmetry, design of the beam injector based on the acceleration section with collinear loads, which aim at implementing layout compactness and high performance, will be introduced in this context.

DESIGN FOR THE LINAC WITH COLLINEAR LOAD

The HUST-FEL-THz Injector

At the HUST-FEL-THz, the booster Linac, which aims at accelerating the beams and driving them out of space-charge-dominated range, has been designed around disk-loaded constant gradient travelling-wave structures. According to the design demands of THz radiation [5], the driving beams should have the energy of about 14 MeV, so that a normal SLAC-like Linac has been adopted to provide adequate acceleration fields. Furthermore, since the beams extracted by the RF gun is still subject to space-charge effects before and in the Linac, as a common solution for emittance compensation, magnetic coils have wrapped around the Linac to provide focusing fields. According to the beam dynamic simulation in physical design of the HUST-FEL-THz injector [7], to obtain sufficient magnetic field strength and adjustment flexibility, a short lens has been placed downstream of the RF gun, and seven pancake-like solenoids cast with epoxy resin have surrounded the Linac. As suggested by Ref. 6, the collinear load based on FeSiAl material has been applied at the Linac to absorb the remnant RF power, so that the sizes of the focusing coils can be reduced. Moreover, comparing with traditional output coupler and waveguide absorbing load, the collinear load is perfectly symmetric which avoids transverse excitation of the beam and intrinsically does not contribute to any emittance growth.

According to the required THz radiation power of the HUST-FEL-THz, the injector must have the ability to work under the beam energy of 14 MeV, the repetition frequency of 50 Hz and the macro-pulse width of 4 μ s. In order to accelerate the beam to 14 MeV within a distance as short as possible, a 19-cell Linac with the constant gradient of about 20.77 MV/m in each cell has been adopted, and a 4-cell collinear load has been set subsequently. Thus, the peak value of input RF power should be 16 MW. For a single load cavity, the input power (P_{in}) and transmitted power (P_{out}) is related by the following relation

$$P_{out} = P_{in} \cdot e^{-2\alpha D} \quad (1)$$

where α is attenuation constant, D is cavity length.

Since the calculated remnant power at the termination of the 14 MeV Linac is 12.10 MW and 5.54 MW with the beam turned-off and turned-on respectively. According to the principle of distribution of average power, to make the

*Corresponding author.

E-mail addresses: TongningHu@hust.edu.cn (T.N. Hu)

remnant RF power be dissipated in the last 4 cells, the collinear load must be designed to have a one-way attenuation of -20 dB. Corresponding power allocations for each cell of the total 24-cell Linac are illustrated in Fig. 1(a), while magnetic field distribution along the Linac is shown in Fig. 1(b).

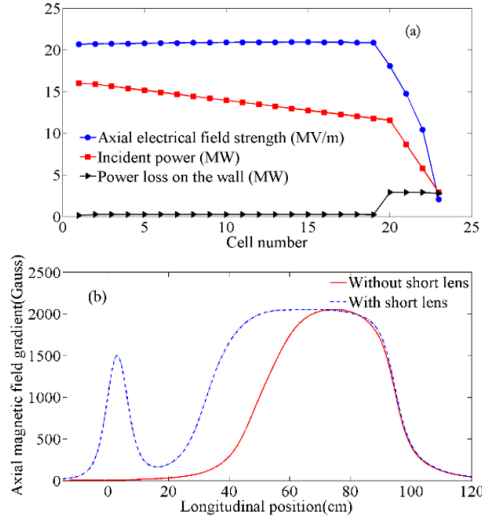


Figure 1: (a) Power and acceleration field distributions along Cell number in the Linac; (b) magnetic field distributions of the focusing coils.

Design of Collinear Load Section

Previous researches [6] show that FeSiAl alloy, the electromagnetic parameters of which are measured to be $\epsilon=114.15-16.96i$, $\mu=1.21-1.90i$, is suitable for the case of high remnant power. Moreover, when the Q -factor of the load cavity is small, the FeSiAl alloy only needs to be coated on the cavity ring.

From Eq. (1) the attenuation factor α is obtained, and the Q -factor of the load cells can be further calculated by the following formula,

$$Q = \frac{\omega}{2V_g \alpha} \quad (2)$$

where V_g is group velocity and is calculated by

$$V_g = \frac{d\omega}{d\beta} = 2\pi D \cdot \frac{df}{d\phi} \quad (3)$$

The upper df is the change of the working frequency of the cavity, and the $d\phi$ is the phase shift of the adjacent accelerating cavity. The performance parameters of the collinear absorbing load under the equal loss power allocation principle obtained by the above steps are shown in Table 1. After determining the Q -factor, thickness and width of the coating material in each cell are determined according to the inverse proportional relationship between Q -factor and the coating volume of FeSiAl alloy material. Then, according to the negative linear relationship between resonant frequency and cavity diameter b , the resonant frequency of the modified cavity is simulated by HFSS Eigen-mode solution to ensure that the resonant frequency is kept at 2856 MHz.

Table 1: Parameters of Load Cavities under the Principle of Distribution of Average Power

Cavity No.	$P_{\text{loss}}(\text{kW})$	α	Q
1	274.29	4.063	622.07
2	274.29	5.699	443.49
3	274.29	9.624	262.62
4	274.29	46.40	54.473

Corrections Considering Thermal Load

Since most of the heat is absorbed by the FeSiAl material on the copper substrate of the cavity, a water cooling system is needed to solve the temperature rise problem to ensure that the accelerator works at about 30°C . The fluid-solid coupling thermal characteristics of the integrated water-cooling system with accelerating tube and collinear load are analyzed by ANSYS. It is found that the temperature field distribution of each cell of the collinear load is not uniform under the principle of distribution of average power and the thermal deformation is also different. That is, the power distribution scheme needs to be optimized. The final simulation results for the optimized power distribution show that the temperature distribution of the four cavities is between $30\sim 32^\circ\text{C}$ and the frequency offset of the cavities is within 30 kHz (Table 2), under the condition that the accelerator working around $30\pm 0.5^\circ\text{C}$. The actual one-way attenuation of the collinear load is about -23.55dB.

Table 2: Temperature Distribution and Frequency Offset of Load Cavities

Cavity No.	Temperature Range($^\circ\text{C}$)	$\Delta b_{\text{avg}}(\mu\text{m})$	Freq Pre(MHz)	Freq After(MHz)	$\Delta f(\text{kHz})$
1	30.064~31.931	0.16	2856.042	2856.013	-29
2	30.523~32.003	0.29	2856.027	2856.003	-24
3	30.710~32.014	0.36	2856.014	2855.996	-18
4	30.427~32.015	0.22	2856.023	2856.011	-12

Table 3: Corrected Collinear Load Parameters after considering Machining Accuracy Error

Cavity No.	b(mm)	m_l(mm)	m_t(mm)	Q	α	P _{loss} (kW)
1	40.834	3.5	0.12	702.99	3.595	246.52
2	40.833	6.0	0.12	418.8	6.035	296.85
3	40.828	10.5	0.12	242.39	10.43	292.58
4	40.810	14.0	0.47	44.218	57.16	267.32

In addition, due to the measurement error and machining accuracy limitations, especially the thickness of FeSiAl alloy coating is about 0.1 mm, so it cannot reach the design value. The actual structure of the load cavity needs to be adjusted on the premise that the microwave physical parameters (such as attenuation coefficient α , Q -factor and resonant frequency f) meet the requirements. The final test cavity parameters after adjustment are shown in Table 3.

EXPERIMENTAL RESULTS

We have used a $2\pi/3$ mode standing wave resonant assembly, as illustrated in Fig. 2(a), to conduct microwave parameter measurements for the collinear load as shown in the Fig. 2(b). Obviously, four TM₀₁ modes, 0, $\pi/3$, $2\pi/3$ and π , can be driven in this structure. The third mode has the same field pattern and characteristics as those in the $2\pi/3$ mode traveling-wave Linac, in which the resonant frequency is 2.856 GHz. In actual experiments, a load cavity would be chosen to replace one of the normal cavities in the resonant assembly.

In order to measure the resonant frequency f and Q -factor of the resonant assembly at $2\pi/3$ mode, a coaxial probe connected to the Network Analyzer is used to transmit and receive signals. The resonant frequency f can be obtained by sweeping the S parameter response curve, and the corresponding frequency at the curve trough is the resonant frequency. To measure the Q -factor, the Critical-Points Method (CPM) [8] is applied to calculate the Q -factor of the resonant assembly through the Smith chart on the Network Analyzer. centred, as far as is possible:

$$Q_0 = \frac{\omega_1 + \omega_2}{2|\omega_1 - \omega_2|} \cdot |x| \approx \frac{f_1 + f_2}{2|f_1 - f_2|}, \text{ for } |x| \approx 1 \quad (4)$$

where f_1 and f_2 are the corresponding frequencies of the reactance extreme points of the impedance circle on the Smith chart.

Because the assembly is simulated in vacuum and the actual measurement is in the atmosphere, it is necessary to correct the measurement error. The resonant frequency f is affected by the relative dielectric constant of air in atmospheric environment as well as the difference between the measuring temperature and the operating temperature of the cavity. The relationship between the frequency f_f in the atmosphere and the frequency f_0 in vacuum is mainly depend on Eq. (5),

$$f_f = \frac{f_0 + \Delta f_T}{\sqrt{\epsilon_r}} = \frac{f_0 + \partial f / \partial T \cdot \Delta T}{\sqrt{\epsilon_r}} \quad (5)$$

where Δf_T is the frequency offset caused by the temperature difference between the measuring and the working temperature, $\partial f / \partial T$ is the rate of change of resonant frequency with cavity temperature, generally taken as $-48 \text{ kHz}/^\circ\text{C}$. ΔT is the difference between the working temperature of the cavity and the testing temperature. ϵ_r is the relative permittivity of air under test conditions, and its empirical formula is as follows:

$$\epsilon_r = 1 + 210 \times 10^{-6} \cdot \frac{P_d}{T} + 180 \times 10^{-6} \cdot \left(1 + \frac{3580}{T}\right) \cdot \frac{P_w}{T} \quad (6)$$

In the above formula, P_d and P_w are the partial pressure of dry gas and water vapor (in torr units) at a certain temperature T respectively, and T is the Kelvin temperature. Finally, the measured value after error correction is shown in Table 4.

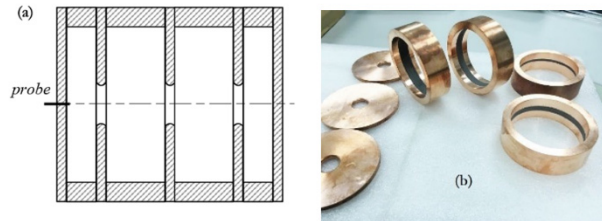


Figure 2: (a) Schematic of a 3-cavity assembly with a feed-in probe; (b) collinear load cavities.

Table 4: The Frequency and Q -factor of the Resonant Assembly Cavities

Cavity No.	Simulation		Measurement	
	Freq(MHz)	Q	Freq(MHz)	Q
1	2854.130	456.395	2854.766	—
2	2854.272	291.685	2854.866	—
3	2854.550	168.144	2856.242	—
4	2855.761	50.079	2856.317	49.901

Finally, it can be seen from the measured data that the processing thickness of the absorbing coating at the first three cavities is thicker than the design value, which makes the volume of FeSiAl material too large, causing that the attenuation of signal is more than expected which leads too much error. Only the Q -factor of the last collinear cavity can be calculated as $Q = 49.901$, which matches the result well. In this case, in order to reduce the deviation between the results and the design values, achieving the desired

Content from this work may be used under the terms of the CC BY 3.0 licence (© 2018). Any distribution of this work must maintain attribution to the author(s), title of the work, publisher, and DOI.

function of the collinear load, it is very important to re-process the thickness of the coating material and the inner diameter of the cavity ring copper base.

The HUST-FEL-THz injector has been constructed since autumn of 2014 [5]. The Linac typically operate at about 20 MV/m, corresponding equipment on-site photo is shown in Fig. 3. After adequate parameter adjustment, the injector can generate high-performance electron beams with the energy of 13.7 MeV, the energy spread of 0.41%, the bunch length of 3.05 ps, and the Nor. Emittance of 8.8 mm mrad, which is more than sufficient to drive the FEL-THz radiation as designed.



Figure 3: The HUST-FEL-THz injector equipment.

As illustrated in Fig.3, the beamline length of the traveling-wave structure with collinear load is only 0.805 m, and the gap between the Linac and the surrounding coils is less than 1 mm.

CONCLUSION

In this context, a SLAC-like traveling wave acceleration tube with collinear load has been described in detail. A

design strategy of simulation combined experiment is proposed. Both theoretic and testing results demonstrates that the final design can achieve a tradeoff between performance and compactness, and involved entire injector can be confined within a very compact scale with facility performance improved by avoiding asymmetric fields.

REFERENCES

- [1] S. Krishnagopal *et al.*, "Free-electron lasers", *Radiation Physics & Chemistry*, vol. 70, pp. 559-569, 2004.
- [2] S. G. Biedron *et al.*, "Compact High-Power Electron Beam Based Terahertz Sources", *Proceedings of the IEEE*, vol. 95, pp. 1666-1678, 2007.
- [3] G. P. Gallerano *et al.*, "Overview of terahertz radiation sources", in *Proc. of the 2004 FEL Conference*, Trieste, Italy, Aug.-Sep. 2004, paper FRBIS02, pp. 216-221.
- [4] H. Hama *et al.*, "Intense coherent terahertz generation from accelerator-based sources", *Nuclear Instruments & Methods in Physics Research A*, vol. 637, pp. 57-61, 2011.
- [5] T. N. Hu *et al.*, "Development of a novel thermionic RF electron gun applied on a compact THz-FEL facility", *Nuclear Instruments & Methods in Physics Research A*, vol. 887, pp. 1-6, 2018.
- [6] Y. Sun *et al.*, "Numerical analysis and design of collinear load for s-band linac based on fesial material", *Nuclear Inst & Methods in Physics Research A*, vol. 623, pp. 883-887, 2010.
- [7] T. N. Hu *et al.*, "Study of beam transverse properties of a thermionic electron gun for application to a compact THz free electron laser", *Review of Scientific Instruments*, vol. 85, pp. 559-569, 2014.
- [8] P. Wang *et al.*, "Accurate characterization of Low-Q microwave resonator using critical-points method", *IEEE Transactions on Microwave Theory & Techniques*, vol. 53, pp. 349-353, 2005.